

# Deformable Image Registration of Follow-Up Breast Magnetic Resonance Images

Tobias Boehler<sup>1</sup>, Kathy Schilling<sup>2</sup>, Ulrich Bick<sup>3</sup>, and Horst K. Hahn<sup>1</sup>

<sup>1</sup> Fraunhofer MEVIS, Bremen 28359, Germany

<sup>2</sup> Boca Raton Community Hospital, FL 33486, USA

<sup>3</sup> Charité Universitätsmedizin, Berlin 10117, Germany

tobias.boehler@mevis.fraunhofer.de

**Abstract.** A novel method for the deformable image registration of follow-up breast magnetic resonance (MR) images is proposed, aimed at an automatic synchronization of temporal images. To compensate potentially large breast deformations and differences among device coordinates, an initial linear alignment of each individual breast, a combination of both transformations using thin-plate splines, as well as a subsequent linear-elastic registration are performed in sequence. Complementary to algorithmic details, an overview of modality-specific factors influencing follow-up registration accuracy is given. The proposed method was evaluated on 20 clinical datasets annotated with landmarks by an expert radiologist. Despite large variations among the MR images, accuracy of the method was sufficient to allow spatial synchronization, with remaining target registration errors of  $< 32\%$ . Concluding, potential enhancements to further increase robustness and accuracy are discussed.

## 1 Introduction

For breast magnetic resonance imaging, comparative examination of currently and previously acquired images provides valuable diagnostic information. Subsequent follow-up imaging and reading take place several months after the preceding acquisition. The temporal interval is chosen patient-specifically. Corresponding consecutive image pairs are also referred to as current-prior images.

Contrary to conventional x-ray mammography (MG), the role of diagnostic software supporting follow-up imaging for breast MRI is less established. Follow-up MR images have complemented MG for long-term classifications of lesions over several years time or to detect potential recurrent diseases [1]. Rather than long-term, short-term follow-up imaging is more frequently applied to assess interventional or medicamentous treatment of lesions by chemotherapy [2,3]. Furthermore, it was shown that additional retrospective follow-up examinations allow the detection of contralateral breast cancers and might even lead to changes in treatment planning and management for early-cancer patients [4]. Moreover, a review of different follow-up schedules has been published recently [5].

The value of follow-up investigations for diagnostics stems from its temporal range: observation of regions of the breast over a longer period of time allows the

radiologist to track pathological and morphological changes in the breast tissue. In particular, such an analysis facilitates the detection of malignant cancers originally graded as “probably benign”. Visual appearance of these cancers often varies significantly over time, so that growth patterns and lesion-typical signs are perceived. These visual cues might then lead to a different rating of the lesion.

In addition, follow-up investigations support the radiologist when some uncertainty with respect to grading remains. Frequently, lesions which are difficult to grade are classified as belonging to BI-RADS category 3, rated as “unclear” or as “probably benign” [6]. For a final assessment of the lesion, a biopsy must be performed. Consequently, the number and expense of evitable biopsies could be reduced by the examination of current-prior images. Routinely and repeatedly conducted follow-up diagnostics are therefore required [7,6].

Registration of follow-up images is complicated by numerous unpredictable factors determined both by breast physiology as well as image acquisition. These issues must be considered in addition to geometric changes of the breast tissue. Table 1 shows the main issues to be regarded. Accordingly, the visual appearance of current and prior images is subject to substantial change.

In particular, tissue deformation, different patient placement and changes of the field-of-view make the reading tedious for the radiologist. Even coarse alignment of such images will therefore offer important support. Spatially-synchronized, simultaneous viewing of current and prior images allows the clinician to quickly establish correspondence between time points and to correlate lesions.















Registration of follow-up MRI is a novel field of research. To our knowledge, only two other contributions have been published before, focused on the quantification of neoadjuvant chemotherapy. Chittineni et al. performed an automatic delineation of the air-breast boundary and chestwall, followed by non-rigid registration [8]. Recently, Li et al. proposed a registration algorithm for short-term follow-up therapy monitoring based on the adaptive bases algorithm [9].

In the following sections, we propose a method that performs an automatic preprocessing and registration of long-term follow-up breast MR images in order to synchronize them. Contrary to [8], no additional segmentation is required. The method extends a previously published registration technique by adding an intermediate thin-plate spline interpolation to ensure consistency of the deformation [10]. We evaluated the method on 20 clinical breast datasets and quantitatively assessed its accuracy using expert-annotated landmark locations. Finally, current limitations and future enhancements of the method are discussed.

## 2 Methods

Application of current-prior registration is a sequential procedure that addresses issues listed in Table 1. In particular, dislocation of the current breast image with respect to the MR device coordinates of the prior image must be compensated. This is achieved by two independent linear image registration tasks, after the breasts have been preprocessed. Remaining local tissue variations are then corrected using non-linear registration to establish further spatial correspondence.

**Table 1.** Overview of patient-specific and general issues for the reading of breast MRI follow-up (current-prior) images, including exemplary images for each described issue. Images courtesy of U. Bick, Charité Berlin.

Issue	Description	Source	Prior image	Current image
Devices	Image characteristics (noise, resolution, in-homogeneities etc.), different breast shapes or larger deformations.	Different coils, different pressure to stabilize the breasts, different MRI scanners, different vendors or technology, change of device coordinate systems.		
Fields-of-view	Either whole thorax, both breasts or single breast (e.g., biopsy imaging), orthogonally reformatted views.	Adjustment of the field-of-view depending on the diagnostic or interventional task, as well as the applied imaging protocol.		
Resolution	Different in-plane and out-of-plane resolutions, as well as voxel size and slice thickness.	Protocol- and device-dependent settings.		
Pathology	Visible lesions or biopsy scars, different appearances in both images.	Interventions, new or recurrent lesions visible in the breast tissue.		
Artifacts	Different MRI artifacts visible in the images.	MR-specific reconstruction artifacts.		
Intensities	Different voxel intensities, local variation and misaligned regions.	Various reasons, such as field inhomogeneities, contrast enhancement, image noise or tissue changes (due to elasticity, relation of fibrotic to adipose or glandular tissue).		
Geometry	Different breast geometry.	Post-interventional (lumpectomy, mastectomy or biopsy) examination of the breast.		

## 2.1 Preprocessing

Initially, each image is divided into two images containing disjunct halves of the breast using an automatic cropping method. The motivation behind this is to perform two separate linear registrations constrained to each breast in order to compensate deformations more effectively. Particularly, different compression applied to each individual breast cannot be modeled by a single affine-linear transformation, since the breast-individual change in pose is frequently dissimilar. The computation of two unconnected transformations is therefore better suited to provide a good initialization for the subsequent linear-elastic image registration. The latter in turn is able to compensate only small non-linear deformations, and therefore requires a preceding alignment.

Consequently, each breast is registered separately after a division of the images. The breasts are separated using a dedicated breast MRI cropping method, which is more accurate in dividing the images than simply splitting along the image centerline [11]. As the reference image  $\mathbf{R}$  for the registration, the follow-up image was selected, whereas the original prior image was taken as the template image  $\mathbf{T}$  to be registered onto the follow-up image. For dynamic contrast-enhanced (DCE) sequences, the first, unenhanced images were selected.

## 2.2 Linear Image Registration

The affine-linear transformation is restricted to a similarity transform with seven degrees of freedom, modeling rotation and translation, as well as isotropic scaling. Therefore, applied transformations retain most of the original breast geometry while allowing deviations from the original size. On the other hand, relative orientation and pose must be modified liberally in order to model different device coordinate systems and independent deformations of each breast.

Assuming that the distribution of glandular, adipose and fibrotic breast tissue remains approximately consistent, intensities of the current and prior images will be closely related. Predominantly, images will be subject to low-frequency intensity changes induced by the breast coil setup. Therefore, it is assumed that the expected intensity change roughly approximates a linear function, and the normalized cross-correlation coefficient

$$e_{ncc}(\mathbf{R}, \mathbf{T}) = 1 - \frac{(\text{cov}(\mathbf{R}, \mathbf{T}))^2}{\sigma^2(\mathbf{R})\sigma^2(\mathbf{T})} \in [0, 1] \quad (1)$$

can be used to measure image dissimilarity [12]. The coefficient is subtracted from unity to assume highest similarity for  $e_{ncc} \rightarrow 0$ . Minimization of equation (1) is achieved by numerical optimization using an iterative Levenberg-Marquardt optimization scheme until convergence is reached [13]. Appropriate iteration step widths are estimated using Armijo's line search strategy [14]. Convergence is declared when suitable stopping criteria are met [15].

Subsequently, deformation fields are computed for each affine-linear registration. To avoid undefined regions of the deformation, the individual fields are

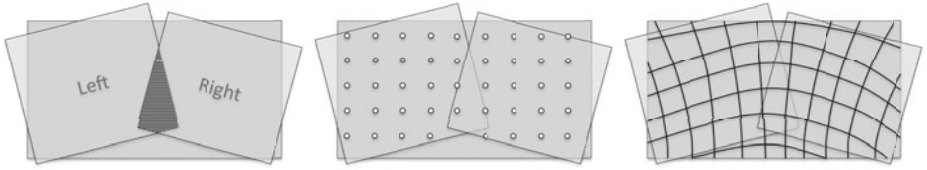


**Fig. 1.** Concatenation of the linear deformation fields. Overlap regions (striped) are neglected (left), and regular grid points are sampled in valid regions (middle). After back-transformation, the two point sets are interpolated using a thin-plate spline transformation, the resulting deformation completely covers the template image (right).

combined to one joint field. However, this combination requires dedicated handling, since the deformation fields are derived from disjunct transformations. Consequently, concatenation by averaging or addition of the two fields will result in a joint field that does not necessarily cover the entire image (see Fig. 1, left). Transformation of the template image with such a deformation will distort the image, because some image regions are not transformed.

Therefore, a thin-plate spline (TPS) interpolation is used to combine both deformation fields and retain a maximum of the original deformations [16]. Although specific poly-affine methods exist [17], the TPS method is employed due to its simplicity and inherent treatment of affine-linear transformations. First, corresponding points before and after linear registration are computed. For this purpose, both breasts and their linear transformations are considered independently to identify point pairs for each transformation. A sparse set of  $n$  and  $m$  regular grid points  $\{\mathbf{p}_i^{left}, \mathbf{p}_j^{right}\} \in \mathbb{R}^3, i = \{1 \dots n\}, j = \{1 \dots m\}$  are defined in regions for which the corresponding deformation field is known, for the left and right breast, respectively. Given the computed homogenous  $4 \times 4$  matrices  $\mathbf{M}^{left}$  and  $\mathbf{M}^{right}$  for each linear transformation, the points (in homogenous notation) are back-projected by left-multiplying the inverse transformations so that

$$\forall i : \mathbf{q}_i^{left} = (\mathbf{M}^{left})^{-1} \mathbf{p}_i^{left} \quad \text{and} \quad \forall j : \mathbf{q}_j^{right} = (\mathbf{M}^{right})^{-1} \mathbf{p}_j^{right} \quad (2)$$

yield the transformed points. Concatenation of the transformed and untransformed point lists creates the two point lists  $\mathbf{P} = \{\mathbf{p}^{left}\} \cup \{\mathbf{p}^{right}\}$  and  $\mathbf{Q} = \{\mathbf{q}^{left}\} \cup \{\mathbf{q}^{right}\}$  with identical sizes  $s = n + m$ . The deformation field is then interpolated using the thin-plate functional

$$u(\mathbf{x}) = \sum_{\nu=1}^4 a_{\nu} \phi_{\nu}(\mathbf{x}) + \sum_{\mu=1}^s w_{\mu} U(|\mathbf{x} - \mathbf{p}_{\mu}|_2) \quad (3)$$

with the 3-D radial basis functions  $U(r) = -\frac{1}{8\pi}r, r \in \mathbb{R}$ , monomials  $\phi_{\nu} \in \mathbb{R}$  and  $\mathbf{p} \in \mathbf{P}$  [18]. Solving for the linear coefficients  $a_{\nu}$  and non-linear coefficients  $w_{\mu}$  in equation (3) using the point set  $\mathbf{Q}$  is achieved by solving an appropriate equation system, using the conjugate gradient method [18]. Subsequently, the dense deformation field can be computed by directly evaluating the functional (3)

at each image coordinate. After interpolation, the resulting joint field contains both the affine-linear deformations as well as intermediate non-linear transitions. The joint field is applied to the original template image and the deformed image is passed as input to the subsequent non-linear deformation.

### 2.3 Linear-Elastic Image Registration

After application of the joint linear transformations, both breasts are roughly aligned. Remaining dissimilarities of image regions are primarily caused by local tissue deformations. For this reason, a linear-elastic transformation model is employed for the non-linear registration [12]. The transformation model enforces the regularization of computed deformations in each iteration similar to the demon’s algorithm [19,20].

For the non-linear registration, a reference image  $\mathbf{R}$  and a template image  $\mathbf{T}$  with  $n$  voxels each are given. For each voxel position  $\mathbf{x}_i \in \mathbb{R}^3, i = 0, \dots, n-1$ , a local non-linear deformation  $\mathbf{u}(\mathbf{x}_i) = (u_x, u_y, u_z)^T$ ,  $\mathbf{u} : \mathbb{R}^3 \rightarrow \mathbb{R}^3$  is computed. The local deformation  $\mathbf{u}(\mathbf{x}_i)$  compensates tissue deformation and is defined by a corresponding displacement field  $\mathbf{u}$ . The local error measure

$$e = \frac{1}{2n} \sum_{i=0}^{n-1} e_{\text{local}}(\mathbf{x}_i, \mathbf{x}_i + \mathbf{u}(\mathbf{x}_i)) \quad (4)$$

depends on the spatial image coordinates  $\mathbf{x}_i$ , the transformed coordinates  $\mathbf{x}_i + \mathbf{u}(\mathbf{x}_i)$ , as well as the reference and template images. Instead of defining a measure of similarity, we thus consider the equivalent minimization of a local error  $e_{\text{local}}$ .

For the linear-elastic registration, an intensity-based similarity measure was selected. The sum of squared differences (SSD) measure is defined as

$$e_{\text{ssd}}(\mathbf{x}_i, \mathbf{x}_i + \mathbf{u}(\mathbf{x}_i)) = [\mathbf{R}(\mathbf{x}_i) - \mathbf{T}(\mathbf{x}_i + \mathbf{u}(\mathbf{x}_i))]^2. \quad (5)$$

Although the measure assumes a constant intensity relation, it was successfully employed in the current-prior registration: Assuming that motion correction has been previously performed, it is sufficient to register only the unenhanced base images. Remaining images are already in the identical coordinate space of the base image. As no local high-frequency temporal enhancement is apparent for these current-prior base image pairs, intensity-based registration is applicable. This does not hold for the global affine-linear registration which considers the entire image. In addition, unlike contrast-enhanced MRI, rapid brightness changes of lesions do not occur. Registration is achieved by minimization of equation (4) using a gradient descent method and explicit Euler integration [20].

To ensure consistency of the computed deformation field, explicit *a posteriori* regularization is employed in each iteration [19,20]. For the registration of breast tissue, regularization with the linear elastic potential defines an appropriate elastic model. An iterative solution was derived by Gramkow [21], employing convolution of the deformation with a linear filter in analogy to the demon’s algorithm [19]. For this purpose, a complex-valued  $7 \times 7 \times 7$  filter-response kernel

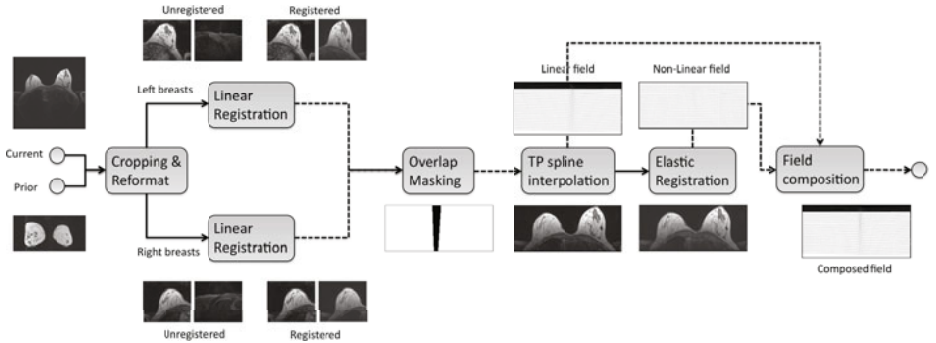


**Fig. 2.** The computational processing pipeline for the proposed method (dashed lines illustrate processing of deformation fields, solid lines image processing)

is generated from the linear-elastic potential [21]. Lamé parameters were set to  $\mu = 500, \lambda = 0.1$ . Convolution of the updated deformation field with the kernel enforces explicit linear-elastic regularization. The deformation is updated by composing it with the update force field, identical to the compositive demon’s algorithm [22]. After the linear-elastic registration has been performed, computed deformations for both linear and non-linear registration need to be composed in order to jointly apply them to the input image. The composed deformation is generated by addition of both deformation fields. Finally, the resulting transformed template image and the composed deformation are stored. The complete image processing scheme is illustrated in Fig. 2.

Synchronization of cursor positions requires that for a selected voxel position  $\mathbf{v} \in \mathbb{R}^3$  in one image a corresponding position  $\hat{\mathbf{v}} \in \mathbb{R}^3$  is computed in the other image. This mapping is defined by the deformation field computed in the previous steps. Given the joint displacement  $\mathbf{u}(\mathbf{v})$  at voxel  $\mathbf{v}$ , we simply compute  $\hat{\mathbf{v}} = \mathbf{v} + \mathbf{u}(\mathbf{v})$  as the corresponding position and reposition the cursor accordingly.

## 2.4 Evaluation

Accuracy of the method was evaluated on clinical datasets, using visual inspection as well as landmark-based measurement of the target registration error [23]. An expert breast radiologist annotated corresponding landmarks in both current and prior images. For this annotation task, a dedicated application had been developed. While the assessment of landmarks alone provides only limited insight into the accuracy of a non-linear image registration, the combination with visual inspection of the registered images allows an overall evaluation. For the visual inspection, reference and template images were inspected as checkerboard-like views. A standalone, synchronized viewing application was evaluated by radiologist experts. Additionally, the deformation fields were displayed as discrete grid overlays, in order to reveal implausible deformations and misregistrations.

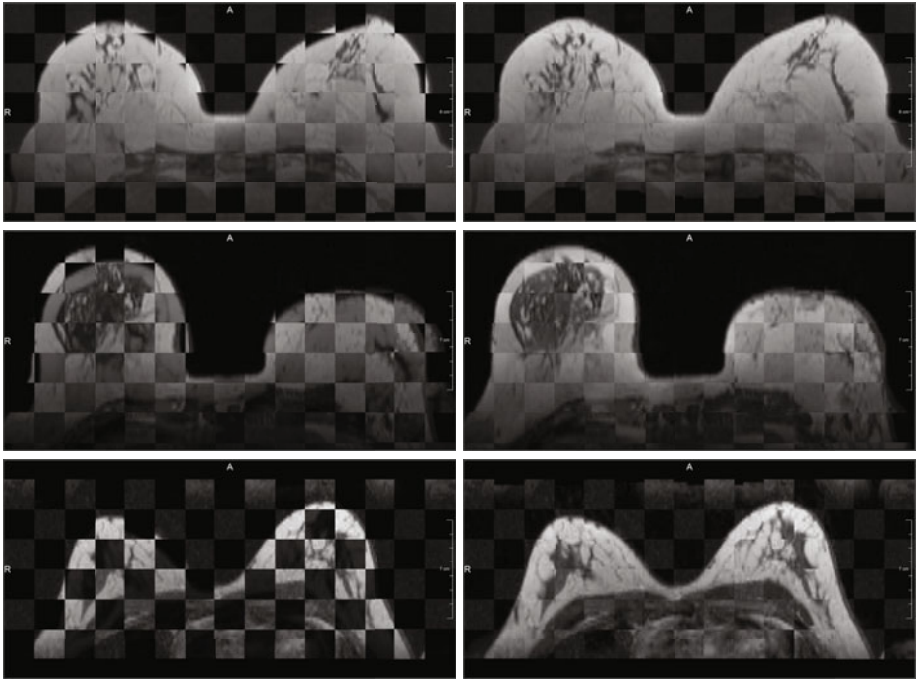


**Fig. 3.** Checkerboard-like overlays of exemplary current-prior images before (left) and after (right) registration with the proposed method. Images courtesy of U. Bick, Charité Berlin.

### 3 Results

The proposed method was evaluated on 20 pairs of clinical T1-weighted MR images acquired from 17 patients using standard DCE protocols and double breast coils. The images were acquired on four different MR scanning systems (Siemens Magnetom and Symphony Vision, Avanto, Sonata) with varying resolutions ( $256 \times 128 \times 64$  to  $560^2 \times 120$  voxels) and voxel sizes ( $1.25^2 \times 2.844mm$  to  $0.625^2 \times 2mm$ ). Biopsy images were removed from the test set prior to processing.

Initially, visual inspection of the current-prior images before and after registration was conducted. The images were displayed to breast radiologists as checkerboard-like overlays. Figure 3 shows three exemplary registration results. After registration, the alignment of internal breast structures and tissue boundaries has improved significantly. Complementarily, the annotated landmarks were transformed with respect to the deformation fields computed by the image registration. In particular, for a given set of reference landmarks, the corresponding transformed reference landmarks were determined. This mapping effectively positions the reference landmarks in the template space. Since a non-symmetric image registration method was applied, the mapping is generally not bijective.



**Table 2.** Resulting distances (in *mm*) between landmarks after registration, including minimum (underlined) and maximum (bold) values

Datasets (1-10)	B1	B2	B3	B4	B5	B6	B7	B8	B9	B10
Mean	7.28	5.88	8.98	12.56	5.41	13.74	6.06	14.02	10.31	16.07
Std.dev.	2.14	0.68	4.23	4.87	1.47	7.53	2.62	6.07	11.09	4.91
Minimum	4.72	4.86	3.6	7.39	3.38	7.02	3.44	7.37	<u>1.35</u>	9.16
Maximum	9.96	6.86	13.94	19.01	6.86	24.25	9.64	22.04	25.94	20.13
Datasets (11-20)	B11	B12	B13	B14	B15	B16	B17	B18	B19	B20
Mean	19.2	12.08	10.36	15.32	16.1	15.35	5.53	<b>24.61</b>	11.37	<u>3.17</u>
Std.dev.	3.21	2.24	4.09	<u>0.32</u>	7.26	7.36	0.72	<b>16.5</b>	7.21	1.55
Minimum	<b>15.4</b>	9.02	5.4	14.91	7.84	9.1	4.52	1.43	5.72	1.44
Maximum	23.25	14.33	15.42	15.69	25.51	25.69	6.14	<b>38.27</b>	21.54	<u>5.2</u>

Euclidean distance measurements were then taken between the mapped reference landmarks and the template landmarks in the template coordinate system. Results of these measurements for the SSD-driven linear-elastic regularizer are shown in Table 2.

For each dataset pair, the average, minimum and maximum distance as well as the standard deviation were computed. Subsequently, average values for all datasets were derived. Overall, the mean distance between landmarks was  $11.67 \pm 5.36mm$ , including all datasets. The minimum average distance was  $3.17mm$ , while the maximum average distance was  $24.64mm$ . The minimum overall distance was  $1.35mm$ , the maximum overall distance  $38.27mm$ . Standard deviations for these values were at  $3.91mm$  and  $8.63mm$ , respectively. Table 3 summarizes the overall distance statistics.

In addition, the relative improvement of landmark distances was estimated by comparison of the original distances with the distances after registration. The resulting values in *mm* and percentages are shown in Table 4. After registration, the mean overall distance was reduced to 31.73% of the original average distance. Standard deviation for the mean values was reduced to 13.36% of its original value. The average minimum and maximum distances were reduced to 27.53% and 35.47% of those for the unregistered images.

**Table 3.** Average distances (in *mm*) over all measurements after registration with the proposed method

Distance ( <i>mm</i> )	Post-registration measurements			
	Mean	Std.dev.	Minimum	Maximum
Mean overall	11.67	4.81	6.53	17.49
Std.dev. overall	5.36	3.97	3.91	8.63
Minimum overall	3.17	0.32	1.35	5.2
Maximum overall	<b>24.64</b>	16.5	15.39	38.27

**Table 4.** Original average distances (in *mm*) over all measurements prior to registration, and relative percentages of the remaining distances after registration

Distance ( <i>mm</i> )	Pre-registration measurements			
	Mean	Std.dev.	Minimum	Maximum
Mean overall	36.77	11.27	23.08	49.3
Std.dev. overall	40.13	18.91	17.43	58.56
Minimum overall	9.56	0.93	4.95	11.73
Maximum overall	159.63	69.72	70.49	240.69
Percentage (%)	Relative remaining distances			
Mean overall	31.74	42.69	27.53	35.47
Std.dev. overall	13.36	21.0	22.43	14.73
Minimum overall	33.15	34.28	27.21	44.33
Maximum overall	15.43	23.66	21.84	15.9

## 4 Discussion

Considering the quantitative and qualitative evaluation, the proposed method effectively reduced the average distance between landmarks to under a third of the original distance. Given the obviously large dislocations and deformations, this reduction greatly improves the spatial correlation. Variation in distance among the set of landmarks was reduced to 13.36% of the original standard deviation, on average. In addition to the reduced minimum and maximum distances, the narrowed range of standard deviations indicates that the registration performed well for the given datasets.

The average distance after registration was 11.67*mm*, compared to 36.77*mm* before processing. Considering the voxel size of  $1.25^2 \times 2$ *mm* for most of the datasets, the achieved improvement already allows to establish synchronization of current and prior datasets. Moreover, the visual inspection of results confirmed that the method aligned images in some cases very accurately.

The method performed worse on datasets containing large changes in breast tissue and geometry, such as post-interventional images. For these datasets, the linear-elastic small-deformation assumption is violated, resulting in imprecise registration results of both the linear and non-linear registrations. Notably, the linear registration often already failed to determine a plausible pre-registration. While the linear-elastic regularization is adequate for small deformations of the breast, its usage for follow-up registration must be supplemented by methods providing custom transformation models to reduce larger variations. Alternatively, diffeomorphic hyper-elastic registration methods must be implemented.

Currently, the non-symmetric mapping of the non-linear registration limits the applicability of the method in that two independent registration tasks need to be performed to allow bidirectional synchronization. A symmetric registration with ensured invertible mapping is currently being developed for this task.

Accuracy of the target registration error measurements depends on the placement of landmark points at feature positions in the images. This annotation is

highly subjective and therefore landmark positions might not be exact, causing larger distance values. Following future evaluations will therefore also consider the fiducial registration error by comparing annotations of multiple experts [23].

## 5 Conclusion

A novel image registration method for the synchronization of breast MRI follow-up images has been proposed, along with an overview of registration-relevant issues. The method was qualitatively and quantitatively evaluated on 20 clinical datasets showing significant variation in breast geometry and image appearance. Accuracy of the registration method in terms of landmark-distances was in the range of  $11.67 \pm 4.81\text{mm}$ , corresponding to a decrease of the initial distances to only 31.74%. Variation was furthermore reduced to 13.36% of the original value. Consequently, the accuracy is sufficient to synchronize follow-up images and support the radiologist during reading. The computationally intensive registration tasks can be precomputed efficiently. At present, the main limitation of the method is the usage of an unspecific linear-elastic image registration method, whose capture range is insufficient for very large deformations of the breast. Therefore, current work aims at improving the method with the integration of prior initialization of the deformation to improve robustness and precision. In addition, the method will be extended to be fully symmetric to ensure an inverse-consistent mapping of the non-linear transformation.

## Acknowledgements

Parts of this work have been funded as part of the HAMAM project by the European Union's 7th Framework Programme, ICT-2007.5.3, grant no. 224538.

## References

1. Kuhl, C., Mielcareck, P., Klaschik, S., Leutner, C., Wardelmann, E., Gieseke, J., Schild, H.: Dynamic Breast MR Imaging: Are Signal Intensity Time Course Data Useful for Differential Diagnosis of Enhancing Lesions? *Radiology* 211(1), 101–110 (1999)
2. Kuhl, C., Schrading, S., Leutner, C., Morakkabati-Spitz, N., Wardelmann, E., Fimmers, R., Kuhn, W., Schild, H.: Mammography, breast ultrasound, and magnetic resonance imaging for surveillance of women at high familial risk for breast cancer. *Journal of Clinical Oncology* 23(33), 8469–8476 (2005)
3. Viehweg, P., Rotter, K., Laniado, M., Lampe, D., Buchmann, J., Kölbl, H., Heywang-Köbrunner, S.: MR imaging of the contralateral breast in patients after breast-conserving therapy. *European Radiology* 14(3), 402–408 (2004)
4. Lehman, C., Gatsonis, C., Kuhl, C., Hendrick, R., Pisano, E., Hanna, L., Peacock, S., Smazal, S., Maki, D., Julian, T., et al.: MRI evaluation of the contralateral breast in women with recently diagnosed breast cancer. *The New England Journal of Medicine* 356(13), 1295–1303 (2007)

5. Montgomery, D., Krupa, K., Cooke, T.: Alternative methods of follow up in breast cancer: a systematic review of the literature. *British Journal of Cancer* 96(11), 1625 (2007)
6. Varas, X., Leborgne, J., Leborgne, F., Mezzera, J., Jaumandreu, S., Leborgne, F.: Revisiting the mammographic follow-up of BI-RADS category 3 lesions. *American Journal of Roentgenology* 179(3), 691–695 (2002)
7. Sickles, E.: Periodic mammographic follow-up of probably benign lesions: results in 3,184 consecutive cases. *Radiology* 179(2), 463–468 (1991)
8. Chittineni, R., Su, M., Nalcioglu, O.: Breast Delineation using Active Contours to Facilitate Coregistration of Serial MRI Studies for Therapy Response Evaluation. In: *IEEE International Conference on Image Processing*, vol. 6, pp. 261–264 (2007)
9. Li, X., Dawant, B., Welch, E., Chakravarthy, A., Freehardt, D., Mayer, I., Kelley, M., Meszoely, I., Gore, J., Yankeelov, T.: A nonrigid registration algorithm for longitudinal breast MR images and the analysis of breast tumor response. *Magnetic Resonance Imaging* 27(9), 1258–1270 (2009)
10. Boehler, T., Bick, U., Hahn, H.: Assessment of image registration for follow-up MR mammography. *European Radiology Supplements* 19(4), 961–963 (2009)
11. Koenig, M., Kohle, S., Peitgen, H.O.: Automatic Cropping of Breast Regions for Registration in MR Mammography. In: *Proceedings of SPIE of Medical Imaging 2005*, pp. 1563–1570 (2005)
12. Modersitzki, J.: *Numerical Methods for Image Registration*. Oxford University Press, New York (2004)
13. Thevenaz, P., Ruttimann, U., Unser, M.: A pyramid approach to subpixel registration based on intensity. *IEEE Transactions on Image Processing* 7(1), 27–41 (1998)
14. Armijo, L.: Minimization of functions having Lipschitz continuous first partial derivatives. *Pacific Journal of Mathematics* 16(1), 1–3 (1966)
15. Gill, P., Murray, W., Wright, M.: *Practical optimization*. Academic Press, London (1981)
16. Bookstein, F.: Principal Warps: Thin-Plate Splines and the Decomposition of Deformations. *IEEE Transactions on Pattern Analysis and Machine Intelligence* 11(6), 567–585 (1989)
17. Commowick, O., Arsigny, V., Isambert, A., Costa, J., Dhermain, F., Bidault, F., Bondiau, P., Ayache, N., Malandain, G.: An efficient locally affine framework for the smooth registration of anatomical structures. *Medical Image Analysis* 12(4), 427–441 (2008)
18. Rohr, K.: *Landmark-based image analysis: using geometric and intensity models*. Kluwer Academic Pub., Dordrecht (2001)
19. Thirion, J.P.: Image Matching as a Diffusion Process: An Analogy with Maxwell's Demons. *Medical Image Analysis* 2(3), 243–260 (1998)
20. Pennec, X., Cachier, P., Ayache, N.: Understanding the Demon's Algorithm: 3D Non-Rigid Registration by Gradient Descent. In: Taylor, C., Colchester, A. (eds.) *MICCAI 1999*. LNCS, vol. 1679, pp. 597–605. Springer, Heidelberg (1999)
21. Gramkow, C., Bro-Nielsen, M.: Comparison of Three Filters in the Solution of the Navier-Stokes Equation in Registration. In: *Proceedings of the Scandinavian Conference on Image Analysis*, pp. 795–802 (1997)
22. Vercauteren, T., Pennec, X., Perchant, A., Ayache, N.: Non-parametric diffeomorphic image registration with the demons algorithm. In: Ayache, N., Ourselin, S., Maeder, A. (eds.) *MICCAI 2007, Part II*. LNCS, vol. 4792, pp. 319–326. Springer, Heidelberg (2007)
23. Hajnal, J., Hawkes, D., Hill, D.: *Medical image registration*. CRC Press, Boca Raton (2001)